Diabetologia (2020) 63:2471–2481
https://doi.org/10.1007/s00125-020-05256-8

ARTICLE

Preserved Ca^{2+} handling and excitation–contraction coupling in muscle fibres from diet-induced obese mice

Francisco Jaque-Fernandez[1] · Agathe Beaulant[2] · Christine Berthier[1] · Laloé Monteiro[1] · Bruno Allard[1] · Mariana Casas[3] · Jennifer Rieusset[2] · Vincent Jacquemond[1]

Received: 4 May 2020 / Accepted: 6 July 2020 / Published online: 25 August 2020

Abstract

Aims/hypothesis Disrupted intracellular Ca^{2+} handling is known to play a role in diabetic cardiomyopathy but it has also been postulated to contribute to obesity- and type 2 diabetes-associated skeletal muscle dysfunction. Still, there is so far very limited functional insight into whether, and if so to what extent, muscular Ca^{2+} homeostasis is affected in this situation, so as to potentially determine or contribute to muscle weakness. In differentiated muscle, force production is under the control of the excitation–contraction coupling process: upon plasma membrane electrical activity, the $Ca_V1.1$ voltage sensor/Ca^{2+} channel in the plasma membrane triggers opening of the ryanodine receptor Ca^{2+} release channel in the sarcoplasmic reticulum (SR) membrane. Opening of the ryanodine receptor triggers the rise in cytosolic Ca^{2+}, which activates contraction while Ca^{2+} uptake by the SR ATPase Ca^{2+}-pump promotes relaxation. These are the core mechanisms underlying the tight control of muscle force by neuronal electrical activity. This study aimed at characterising their inherent physiological function in a diet-induced mouse model of obesity and type 2 diabetes.

Methods Intact muscle fibres were isolated from mice fed either with a standard chow diet or with a high-fat, high-sucrose diet generating obesity, insulin resistance and glucose intolerance. Properties of muscle fibres were investigated with a combination of whole-cell voltage-clamp electrophysiology and confocal fluorescence imaging. The integrity and density of the plasma membrane network (transverse tubules) that carries the membrane excitation throughout the muscle fibres was assessed with the dye Di-8-ANEPPS. $Ca_V1.1$ Ca^{2+} channel activity was studied by measuring the changes in current across the plasma membrane elicited by voltage-clamp depolarising pulses of increasing amplitude. SR Ca^{2+} release through ryanodine receptors was simultaneously detected with the Ca^{2+}-sensitive dye Rhod-2 in the cytosol. $Ca_V1.1$ voltage-sensing activity was separately characterised from the properties of intra-plasma-membrane charge movement produced by short voltage-clamp depolarising pulses. Spontaneous Ca^{2+} release at rest was assessed with the Ca^{2+}-sensitive dye Fluo-4. The rate of SR Ca^{2+} uptake was assessed from the time course of cytosolic Ca^{2+} recovery after the end of voltage excitation using the Ca^{2+}-sensitive dye Fluo-4FF. The response to a fatigue-stimulation protocol was determined from the time course of decline of the peak Fluo-4FF Ca^{2+} transients elicited by 30 trains of 5-ms-long depolarising pulses delivered at 100 Hz.

Results The transverse tubule network architecture and density were well preserved in the fibres from the obese mice. The $Ca_V1.1$ Ca^{2+} current and voltage-sensing properties were also largely unaffected with mean values for maximum conductance and maximum amount of charge of 234 ± 12 S/F and 30.7 ± 1.6 nC/μF compared with 196 ± 13 S/F and 32.9 ± 2.0 nC/μF in fibres from mice fed with the standard diet, respectively. Voltage-activated SR Ca^{2+} release through ryanodine receptors also exhibited very similar properties in the two groups with mean values for maximum rate of Ca^{2+} release of 76.0 ± 6.5 and 78.1 ± 4.4 μmol l^{-1} ms^{-1}, in fibres from control and obese mice, respectively. The response to a fatigue protocol was also largely unaffected in fibres from the obese mice, and so were the rate of cytosolic Ca^{2+} removal and the spontaneous Ca^{2+} release activity at rest.

✉ Vincent Jacquemond
vincent.jacquemond@univ-lyon1.fr

[1] Institut NeuroMyoGène, UMR CNRS 5310 – Inserm U1217 – Université Claude Bernard Lyon 1 – Univ Lyon, Faculté de Médecine et de Pharmacie, Lyon, France

[2] CarMeN Laboratory, Inserm, INRA, INSA Lyon, Université Claude Bernard Lyon 1 – Univ Lyon, Pierre-Bénite, France

[3] Programa de Fisiología y Biofísica, Instituto de Ciencias Biomédicas, Facultad de Medicina, Universidad de Chile, Santiago, Chile

Research in context

What is already known about this subject?

- Obesity and type 2 diabetes are associated with skeletal muscle dysfunction
- A high-fat diet induces a decrease in specific muscle force production

What is the key question?

- Does impaired Ca^{2+} homeostasis contribute to skeletal muscle dysfunction and weakness in a mouse model of obesity and type 2 diabetes?

What are the new findings?

- Ca^{2+} entry and voltage-sensing steps of excitation–contraction coupling at the plasma membrane level are unaffected in muscle fibres from obese mice
- Properties of intracellular Ca^{2+} handling by the sarcoplasmic reticulum are also completely preserved in muscle fibres from obese mice

How might this impact on clinical practice in the foreseeable future?

- The Ca^{2+} handling capacities of skeletal muscle that allow control of force production are intact in a mouse model of obesity and type 2 diabetes. These findings are important for our understanding of muscle function/dysfunction and may impact on clinical practice in relation to physical exercise in individuals with obesity or diabetes

Conclusions/interpretation The functional properties of the main mechanisms involved in the control of muscle Ca^{2+} homeostasis are well preserved in muscle fibres from obese mice, at the level of both the plasma membrane and of the SR. We conclude that intracellular Ca^{2+} handling and excitation–contraction coupling in skeletal muscle fibres are not primary targets of obesity and type 2 diabetes.

Keywords Ca^{2+} homeostasis · Cytosolic Ca^{2+} clearance · Excitation–contraction coupling · Obesity · Ryanodine receptor · Sarcoplasmic reticulum Ca^{2+} release · Skeletal muscle · Type 2 diabetes

Abbreviations

BTS	*N*-benzyl-*p*-toluene sulphonamide
$[Ca_{Tot}]$	Total amount of released Ca^{2+} referred to the myoplasmic water volume
$d[Ca_{Tot}]/dt$	Rate of SR Ca^{2+} release
ECC	Excitation–contraction coupling
F_0	Baseline fluorescence
FDB	Flexor digitorum brevis
G_{max}	Maximum conductance
HFD	High-fat diet
HFHSD	High-fat, high-sucrose diet
k	Steepness factor
Q_{max}	Maximum charge
RYR1	Type 1 ryanodine receptor
SCD	Standard chow diet
SERCA	Sarco/endoplasmic reticulum Ca-ATPase
SR	Sarcoplasmic reticulum
T-tubule	Transverse tubule
$V_{0.5}$	Half-activation potential
V_{rev}	Apparent reversal potential

Introduction

Obesity and its deleterious complications, insulin resistance and type 2 diabetes mellitus, are associated with skeletal muscle dysfunction [1, 2]. Long-term systemic impairments related to the disease status such as cardiomyopathy, peripheral neuropathy and vascular disease eventually contribute but there is also evidence that the muscle tissue itself suffers from inherently reduced performance. Still, underlying mechanisms remain unclear and the situation is also complicated by concomitant processes operating to adapt muscle function to overweight-induced increased force demand. The literature related to altered muscle function in obesity and diabetes is intricate because of the diversity of experimental conditions and animal models used to tackle this issue, including a variety of genetically-modified murine models, selected murine strains, and pharmacological- or dietary-induction protocols [3, 4]. If one focuses on the most common reason for obesity and type 2 diabetes in humans, diet-induced obesity in animal models may be considered of somewhat more specific

interest. Accordingly, there is reproducible evidence that a sufficiently long period (≥10 weeks) of high-fat diet (HFD) induces a decrease in specific force production, as assessed ex vivo from mouse muscle [5–7].

Altered intracellular Ca^{2+} handling contributes to obesity-induced cardiac dysfunction [8, 9] (see for review [10, 11]). Skeletal muscle function critically depends upon stringent control of intracellular Ca^{2+} with three proteins playing a key role in this process: $Ca_V1.1$ (a voltage sensor and Ca^{2+} channel in the transverse tubule [T-tubule] membrane), type 1 ryanodine receptor (RYR1; the Ca^{2+} release channel in the sarcoplasmic reticulum [SR] membrane), and sarco/endoplasmic reticulum Ca-ATPase (SERCA; the SR Ca^{2+} ATPase), ensuring Ca^{2+} uptake and consequent cytosolic Ca^{2+} clearance. Muscle force is triggered by cytosolic Ca^{2+} increase, promoting Ca^{2+} binding to troponin C. This occurs when T-tubule depolarisation sensed by $Ca_V1.1$ is transduced into opening of RYR1 channels and consequent SR Ca^{2+} release: the excitation–contraction coupling (ECC) process [12–15]. Besides activation of force, intracellular Ca^{2+} also plays a key role in other aspects of muscle function including metabolism and signalling cascades involved in gene expression [16, 17], processes that may also be modified because of altered Ca^{2+} homeostasis. Altogether, there is thus strong interest in determining whether functional aspects of Ca^{2+} homeostasis are affected in diet-induced obesity. Surprisingly, this has been largely experimentally overlooked so far, at least at the level of intact muscle fibres under membrane voltage control, a condition made essential by the stringent command exerted by plasma membrane voltage on intracellular Ca^{2+} homeostasis. In other words, no quantitative characterisation of the functional features of Ca^{2+} handling at the physiological millisecond time range of activation of ECC is available in this disease situation. This is at odds with the fact that potential mechanisms involved in Ca^{2+} dysregulation and target mechanisms have been largely highlighted in the literature [2, 18].

We have used single muscle fibres isolated from mice fed with a high-fat, high-sucrose diet (HFHSD) generating obesity, hyperinsulinaemia, insulin resistance and glucose intolerance [19] to perform an extensive functional characterisation of intracellular Ca^{2+} signalling and ECC in that situation.

Methods

All experiments and procedures were performed according to the ethics principles of the French Department of Veterinary Services and the French Ministry for Higher Education, Research and Innovation, in accordance with the guidelines of the local animal ethics committee of the University Claude Bernard Lyon 1, the French Ministry of Agriculture (decree 87/848), and the revised European Directive 2010/63/EU. The experimental protocol of diet-induced obesity was approved by the Animal Experimentation Committee no. C2EA-15 of the Rhône-Alpes Region. Experiments were performed at room temperature (20–22°C).

HFHSD-induced diabetic mice Four-week-old C57BL/6JOlaHsd male mice were purchased from ENVIGO (Gannat, France) and housed at 22°C with a 12 h light/dark cycle. Following delivery, mice were distributed within cages and left for 1 week to adapt to the new environment. Cages were then allocated to 2 groups: one with free access to a standard chow diet (SCD) (Rod16-A, Genobios: 16.9% protein, 4.3% lipids, 55.5% carbohydrate essentially from starch with no sucrose added) and the other with free access to a pelleted HFHSD diet (260HF U8978 version 19; SAFE; 20% protein, 36% lipids, 37% carbohydrate including 14.5% starch and 17.9% sucrose) for 16 weeks as described previously [19]. For simplicity, mice, and fibres isolated from the mice in the two groups, are referred to as SCD and HFHSD. Two sets of five mice of each group were used in this study. The first set was dedicated to characterisation of T-tubule membrane architecture, voltage-activated Ca^{2+} current and intracellular Ca^{2+} transients, and spontaneous Ca^{2+} release events at rest. In the second set we measured intramembrane charge movement and spontaneous Ca^{2+} release events. In the first group, body mass and blood glucose were assessed twice a week and a GTT and ITT were performed during weeks 4, 8, 12 and 16 after the beginning of the diet, as previously described [19]. In the second group an ITT and GTT were performed during week 15. In all mice, body weight and blood glucose were assessed before euthanasia. Immediately following euthanasia, prior to the preparation of isolated muscle fibres (see next section), the gastrocnemius muscles, the heart, the liver and the white adipose tissue were removed and weighed.

Preparation of isolated muscle fibres Single fibres from the flexor digitorum brevis (FDB) and interosseus muscles were isolated as previously described [20]: mice were anaesthetised with isoflurane and killed by cervical dislocation before removal of the muscles. Muscles were incubated in Tyrode's solution containing 2 mg/ml collagenase (Sigma, type 1) for 60 min at 37°C. Single fibres were obtained by mechanical trituration within a culture μ-dish (Ibidi, Planegg/Martinsried, Germany) filled with culture medium containing 10% FBS (MI199; Eurobio, France), the bottom of which had been first coated with a thin layer of silicone. Isolated fibres settled on the silicone surface and were then embedded with additional silicone so that only a portion of the fibre extremity remained in contact with the extracellular medium. The initial silicone coating of the chamber bottom was necessary because of the hydrophobic nature of the silicone grease, which makes it very hard to adhere to a solid substrate in a liquid environment. The

silicone grease we used was SILBIONE Paste 70,428 (Elkem Silicones, Saint-Fons, France).

Electrophysiology Voltage-clamp experiments were performed on FDB muscle fibres using a micropipette filled with an intracellular-like medium (see Methods: Buffers and incubation media). The pipette tip was inserted into the silicone-insulated part of the fibre and was gently crushed against the chamber bottom to ease dialysis and reduce series resistance. Composition of the extracellular solution and of the pipette solution were adapted to the experiment type (see Methods: Buffers and incubation media). The fibre interior was dialysed for 30 min to allow for intracellular equilibration of the solution before starting measurements. The chlorided silver wire inside the pipette was connected to an RK-400 patch-clamp amplifier (Bio-Logic, Claix, France) in whole-cell configuration, in combination with an analogue–digital converter (Digidata 1440A, Axon Instruments, Foster City, CA, USA) controlled by pClamp 9 software (Axon Instruments). The effective series resistance was further decreased by analogue compensation. Unless otherwise specified, the holding voltage was set to −80 mV.

$Ca_V1.1$ Ca^{2+} current was measured in response to 0.5-s-long depolarising steps. The linear leak component of the current was removed by subtracting the adequately scaled value of the current measured during a −20 mV step. This subtraction did not fully eliminate the outward current measured during pulses to values between −50 and − 30 mV, below the threshold of activation of the Ca^{2+} current. In order to correct for this, the voltage-dependence of the values for the residual current was fitted by a linear function from −50 to −30 mV; the fit was extrapolated to the entire range of voltage values and fitted values were subtracted from the measured values for peak $Ca_V1.1$ current. The voltage-dependence of peak current values (normalised to the capacitance), was fitted with the following equation:

$$I(V) = G_{max}(V-V_{rev})/(1 + \exp(V_{0.5}-V)/k])$$

with $I(V)$ the peak current density at the command voltage V, G_{max} the maximum conductance, V_{rev} the apparent reversal potential, $V_{0.5}$ the half-activation potential (also commonly referred to as voltage of equal charge distribution) and k the steepness factor. As for the values of peak Ca^{2+} current, values for G_{max} were also expressed normalised to the capacitance (S/F).

$Ca_V1.1$ charge movement currents were measured from a holding voltage of −100 mV and analysed as previously described [21, 22]. In brief, adequately scaled control records elicited by 25-ms-long pulses of −20 mV were subtracted from the current elicited by test depolarising pulses of the same duration to various levels [23]. The amount of charge moved during a test pulse was measured by integrating the on and off portions of the corrected test current records. The steady-state distribution of charge (normalised to fibre capacitance) was fitted with a two-state Boltzmann function:

$$Q(V) = Q_{max}/(1 + \exp[(V_{0.5}-V)/k])$$

with Q_{max} the maximal available charge, $V_{0.5}$ the voltage of equal charge distribution and k the steepness factor.

Confocal imaging Confocal imaging was conducted with a Zeiss LSM 5 Exciter equipped with a ×63 oil immersion objective (numerical aperture 1.4). For detection of Rhod-2 and Fluo-4FF fluorescence, excitation was from the 543 nm line of a HeNe laser and from the 488 nm line of an Argon laser, respectively, and fluorescence was collected above 560 nm and above 505 nm, respectively. Rhod-2 and Fluo-4FF fluorescence changes were imaged using the line-scan mode (x,t) of the system and expressed as F/F_0 where F_0 is the baseline fluorescence. Quantification of the Ca^{2+} release flux underlying the Rhod-2 Ca^{2+} transients was performed as previously described [24]. In each fibre, the voltage-dependence of the peak rate of Ca^{2+} release was fitted with a Boltzmann function.

Di-8-ANEPPS and Fluo-4 fluorescence were collected above 505 nm with 488 nm excitation. For imaging the T-tubule network, interosseus muscle fibres were incubated for 30 min in the presence of 10 μmol/l Di-8-ANEPPS. The T-tubule density was estimated as described previously [24].

For Ca^{2+} sparks measurements, interosseus muscle fibres were incubated for 30 min in the presence of 10 μmol/l Fluo-4 acetoxymethyl ester (AM). Thirty consecutive confocal frames of Fluo-4 fluorescence (102.4 × 102.4 μm, 989 ms per frame) were acquired in each fibre. To quantify the Ca^{2+} sparks activity, images in the stack were smoothed and the standard deviation of fluorescence intensity at each pixel position, along the stack, was calculated. The 20% largest values in the standard deviation image were removed to calculate the mean standard deviation of silent areas. The active area was then defined as pixel positions exhibiting at least 1.5 × larger values of standard deviation than the mean standard deviation value from silent areas.

Buffers and incubation media Tyrode solution contained (in mmol/l) 140 NaCl, 5 KCl, 2.5 $CaCl_2$, 2 $MgCl_2$, 10 HEPES. The extracellular solution for measurements of $Ca_V1.1$ Ca^{2+} current and Ca^{2+} transients contained (in mmol/l) 140 tetraethylammonium-methanesulfonate, 2.5 $CaCl_2$, 2 $MgCl_2$, 1 4-aminopyridine, 10 HEPES and 0.002 tetrodotoxin. For measurements of Fluo-4FF Ca^{2+} transients, it also contained 0.05 *N*-benzyl-*p*-toluene sulphonamide (BTS) to block contraction. The pipette solution contained (in mmol/l) 120 K-glutamate, 5 Na_2-ATP, 5 Na_2-phosphocreatine, 5.5 $MgCl_2$, 5 glucose, 5 HEPES. For measurements of Rhod-2 and Fluo-4FF Ca^{2+} transients it also contained 15 EGTA, 6 $CaCl_2$, 0.1 Rhod-2, and 0.1 Fluo-4FF, respectively.

For measurements of $Ca_V1.1$ charge movement the extracellular solution contained (in mmol/l) 140 tetraethylammonium (TEA)-methanesulfonate, 0.1 $CaCl_2$, 3 $MgCl_2$, 1 $CdCl_2$, 0.5 $MnCl_2$, 1 4-aminopyridine, 0.5 9-anthracene-carboxylic acid, 10 HEPES and 0.002 tetrodotoxin and fibres were dialysed through the pipette with a solution containing (in mmol/l) 140 TEA-methanesulfonate, 5 Na_2-ATP, 5 Na_2-phosphocreatine, 5.5 $MgCl_2$, 5 glucose, 5 HEPES. BTS was purchased from Tocris Bioscience (Bio-Techne, Lille, France). All fluorescent indicators were purchased from Thermo Fisher Scientific (Illkirch, France). All solutions were adjusted to pH 7.20.

Statistics No randomisation procedure was carried out. Experimenters were not blind to group assignment and outcome assessment. Statistical analysis was performed with Origin 8.0. Data values are presented as mean ± SEM for *n* fibres. Statistical significance was determined using two-tailed Student's *t* tests comparing the means ($*p \leq 0.05$).

With respect to results shown in Fig. 3, data from one muscle fibre in the SCD group and from one muscle fibre in the HFHSD group were excluded because in both cases the fit to the peak Ca^{2+} current versus voltage data gave non-rational values for maximal conductance (~10 times less than the mean value) and apparent reversal potential (more than 80 mV more positive than the mean value). Muscle fibres from one mouse initially scheduled for the SCD group could not be used because of an experimental mistake during the protocol of incubation at 37°C in the presence of collagenase.

Results

Obesity, insulin resistance and glucose intolerance in the HFHSD mice The status of our animals over the course of the diet protocol is shown in Fig. 1, as assessed from the first group of mice (see Methods: HFHSD-induced diabetic mice). At the end, the body weight of the HFHSD animals was ~1.7 times that of SCD ones (Fig. 1a); mean values for body weight at the end of the diet protocol for SCD and HFHSD animals were 28.6 ± 0.5 g ($n = 9$) and 50.1 ± 0.9 g ($n = 9$) ($p < 0.0001$), respectively. There was no associated change in the weight of the gastrocnemius (0.17 ± 0.01 g, $n = 9$ and 0.21 ± 0.02 g, $n = 9$; $p = 0.14$) nor of the heart (0.17 ± 0.01 g, $n = 9$ and 0.21 ± 0.02 g, $n = 9$; $p = 0.09$), whereas the weight of the liver (1.30 ± 0.04 g, $n = 9$ and 3.11 ± 0.34 g, $n = 9$; $p < 0.0001$) and of the white adipose tissue (measured as the epididymal adipose tissue: 0.51 ± 0.04 g, $n = 9$ and 2.06 ± 0.17 g, $n = 9$; $p < 0.0001$) were substantially increased in HFHSD vs SCD animals, respectively. Results from GTT and ITT performed at weeks 4, 8, 12 and 16 are shown in Fig. 1b and c, respectively: HFHSD mice maintained an elevated blood glucose level following injection of either glucose or insulin: from the 10 min time point following either glucose or insulin injection, the mean glucose level in HFHSD mice ranged between approximately 1.5 and 2.3 times the level in SCD mice (the difference being statistically significant between the two groups at any time point of the four sets of measurements), establishing the glucose intolerance and the systemic insulin resistance, and thus the diabetic status generated by the protocol.

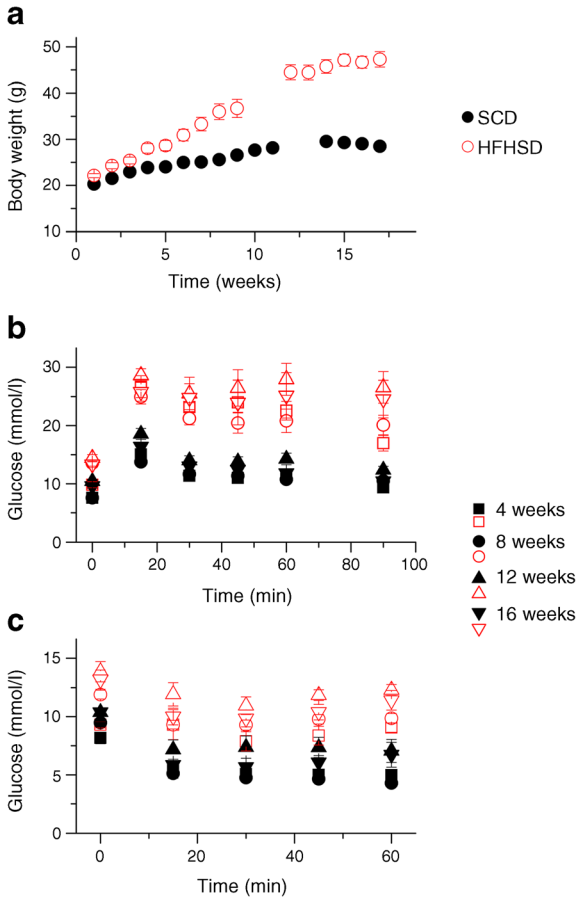

Fig. 1 Body mass, GTT and ITT in SCD and HFHSD mice. (**a**) Mean values for body weight of SCD ($n = 9$) and HFHSD mice ($n = 9$), over the course of the diet protocol. The gaps in the SCD and HFHSD data are due to a short break in data collection. (**b**, **c**), Mean values for blood glucose concentration before ($t = 0$) and after intraperitoneal injection of either 2 mg/g glucose (**b**) or 0.75 U/kg insulin (**c**). Measurements were performed at weeks 4, 8, 12 and 16 after the beginning of the diet. (**b**, **c**) When comparing the mean glucose level between the SCD and HFHSD groups at any given time point of the GTT protocol (**b**) using a *t* test, comparisons all had $p < 0.01$ (at 4, 8 and 12 weeks) and $p < 0.02$ (at 16 weeks); when comparing the mean glucose level between the SCD group and the HFHSD group at any given time point of the ITT protocol (**c**) using a *t* test, comparisons all had $p < 0.02$ (at 4, 12 and 16 weeks) and $p < 0.001$ (at 8 weeks). Data are mean ± SEM

T-tubule network and passive electrical properties in SCD and HFHSD muscle fibres The T-tubule membrane system plays a critical role in ECC and in glucose transport and HFD may enhance its cholesterol content [25] with potential adverse

consequences for T-tubule integrity and function [26, 27]. We labelled the plasma membrane of fibres with Di-8-ANEPPS. Corresponding *x,y* confocal images from SCD (Fig. 2a, c) and HFHSD muscle fibres (Fig. 2b, d) showed no sign of alteration of the network in the HFHSD group and the transverse profile of fluorescence showed the expected double-peak pattern characteristic of T-tubule organisation in mammalian muscle (graphs in Fig. 2c, d). Analysis of Di-8-ANEPPS images collected from 20 muscle fibres from two SCD mice and from 30 fibres from three HFHDS mice showed no change in T-tubule density (Fig. 2e), but, incidentally, the mean value for sarcomere length was slightly but significantly reduced in the HFHSD compared with the SCD group (2.04 ± 0.01 vs 2.11 ± 0.02; $p = 0.001$; Fig. 2f). Preservation of the T-system in the HFHSD fibres was confirmed by the passive electrical properties of the fibres: membrane current records

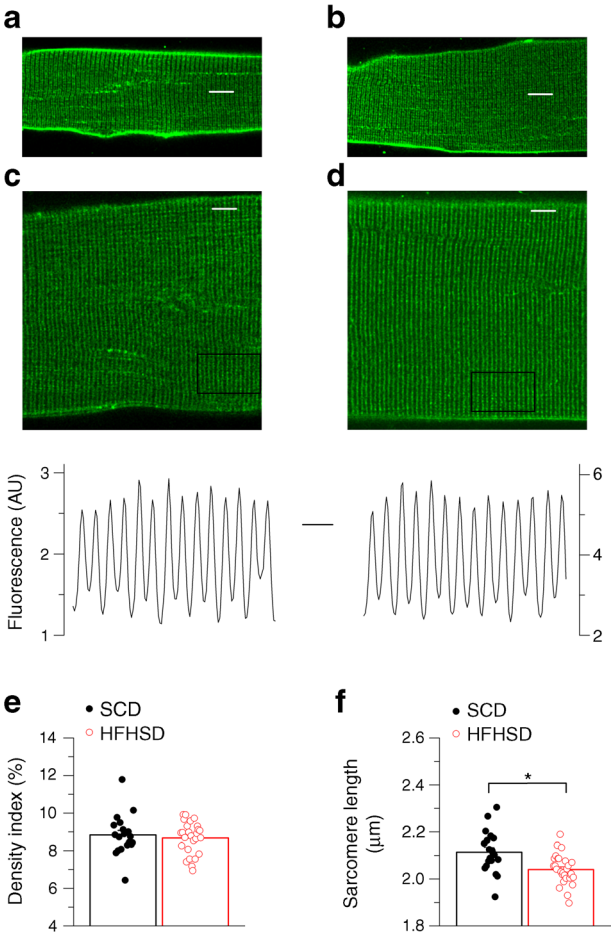

Fig. 2 T-tubule system network. (**a**–**d**) *x,y* confocal images of Di-8-ANNEPS fluorescence from separate SCD (**a**, **c**) and HFHSD muscle fibres (**b**, **d**) at two different magnifications (**a**, **b**: scale bar, 10 μm; **c**, **d**: scale bar, 5 μm). (**c**, **d**) Graphs show the transverse pattern of Di-8-ANNEPS fluorescence (scale bar, 2 μm) over the region shown with a box in the corresponding *x,y* images above. AU, arbitrary unit.(**e**, **f**) Mean values for T-tubule density index and for sarcomere length in the SCD ($n = 20$ fibres from 2 mice) and HFHSD ($n = 30$ fibres from 3 mice) groups. Data are mean ± SEM. *$p < 0.05$

from fibres used to measure $Ca_V1.1$ Ca^{2+} current gave mean values for capacitance and input resistance of 949.0 ± 68 and 930.6 ± 61 pF, and 11.9 ± 1 and 12.5 ± 0.8 MΩ, in the SCD group ($n = 21$ fibres from four mice) and in the HFHSD group ($n = 30$ fibres from five mice), respectively. Because mean values for fibre diameter did not differ between the SCD (44.8 ± 1.4 μm) and HFHSD group (43.4 ± 1.4 μm) and assuming that a fibre portion of similar length was always under voltage-clamp, results establish that the T-tubule network is preserved in the obesity situation.

$Ca_V1.1$ Ca^{2+} current and voltage-sensing properties in SCD and HFHSD muscle fibres $Ca_V1.1$ is the most well-identified and characterised Ca^{2+} entry pathway across the plasma/T-tubule membrane of muscle fibres. Example $Ca_V1.1$ Ca^{2+} current records from an SCD and from an HFHSD muscle fibre are shown in Fig. 3a and b, respectively; mean values for peak Ca^{2+} current vs voltage in the two groups are shown in Fig. 3c whereas mean values for the parameters obtained from fitting each individual peak current vs voltage relationship are shown in Fig. 3d–g. There was no significant change in any parameter in the HFHSD group. Mean values for maximum conductance were 196 ± 13 S/F and 234 ± 12 S/F in fibres from the SCD and from the HFHSD group, respectively.

$Ca_V1.1$ also exerts the critical function of coupling the T-tubule depolarisation to RYR1 Ca^{2+} channel activation in the SR membrane. $Ca_V1.1$ voltage-sensing function was assessed from intramembrane charge movement. Example traces of charge current from an SCD and from an HFHSD muscle fibre are shown in Fig. 4a whereas mean values for the amount of charge vs voltage are shown in Fig. 4b (data from 22 SCD fibres and 21 HFHSD fibres, each from three mice in each group). Properties of charge movement were similar in SCD and HFHSD muscle fibres (Fig. 4c–e), with mean values for maximum amount of charge of 32.9 ± 2.0 and 30.7 ± 1.6 nC/μF, respectively. This demonstrates that the amount of $Ca_V1.1$ in the plasma/T-tubule membrane and its voltage-sensing properties are preserved in this situation.

Voltage-activated SR Ca^{2+} release Properties of RYR1 channels activity upon fibre activation were assessed from voltage-clamp-activated cytosolic Ca^{2+} transients. A family of such F/F_0 Rhod-2 transients from an SCD and an HFHSD muscle fibre are shown in Fig. 5a and b, respectively, while traces for the corresponding calculated rate of SR Ca^{2+} release are shown in Fig. 5c and d, respectively. As classically reported in this preparation, the time course of SR Ca^{2+} release exhibits an early peak followed by a decay towards a much lower level. There was no obvious qualitative feature of the Rhod-2 transients and of the rate of Ca^{2+} release that differed between SCD and HFHSD fibres. This was confirmed by the analysis showing that neither mean values for peak rate of SR Ca^{2+}

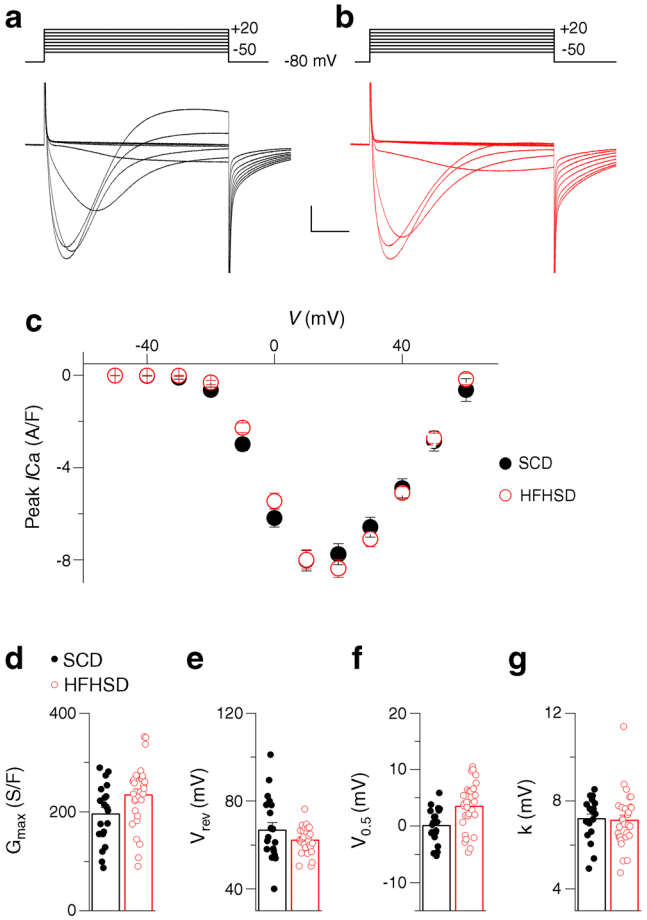

Fig. 3 $Ca_V1.1$ Ca^{2+} current. (**a**, **b**) example traces of Ca^{2+} current in an SCD (**a**) and in an HFHSD muscle fibre (**b**) in response to the voltage-clamp pulse protocol shown at the top. Horizontal axis, time (scale bar 100 ms), vertical axis, current (scale bar 2 A/F). (**c**) Mean values for the peak Ca^{2+} current density vs voltage in the SCD ($n = 20$ fibres from 4 mice) and HFHSD ($n = 29$ fibres from 5 mice) groups. (**d**–**g**) Corresponding mean values for the parameters obtained from fitting each individual peak current vs voltage relationship with the appropriate function (see Methods: Electrophysiology). Data are mean ± SEM

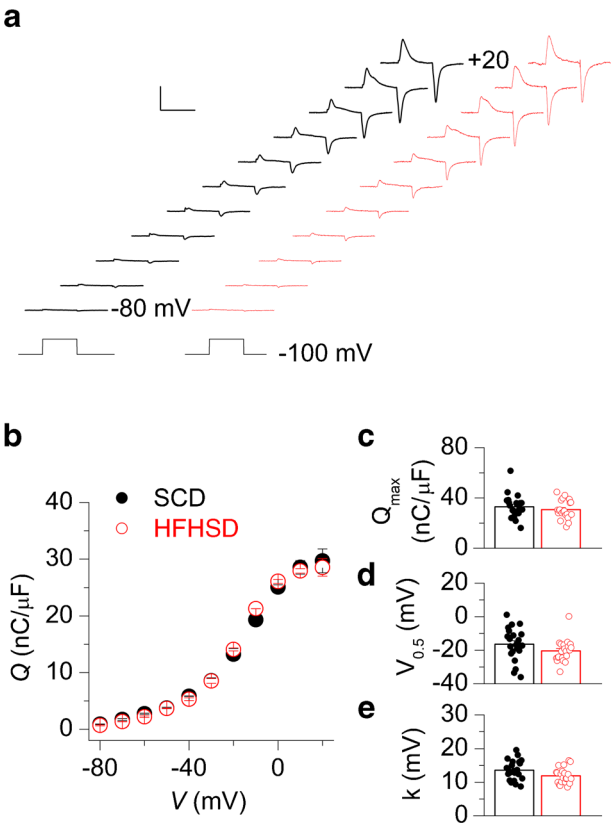

Fig. 4 $Ca_V1.1$ charge movement. (**a**) example traces of $Ca_V1.1$ charge movement currents in an SCD (left, black) and in an HFHSD muscle fibre (right, red) in response to voltage-clamp depolarising pulses from −100 mV to values ranging between −80 and +20 mV. Horizontal axis, time (scale bar 25 ms), vertical axis, current (scale bar 5 A/F). (**b**) Mean values for the $Ca_V1.1$ charge density vs voltage in the SCD ($n = 22$ fibres from 3 mice) and HFHSD ($n = 21$ fibres from 3 mice) groups. (**c**–**e**) Mean values for the parameters obtained from fitting each individual charge vs voltage relationship with the appropriate function (see Methods: Electrophysiology). Data are mean ± SEM

release (peak $d[Ca_{Tot}]/dt$, Fig. 5e), nor for its time to peak (t_{peak}, Fig. 5g) nor for total amount of released Ca^{2+} ($[Ca_{Tot}]$ calculated from the time integral of the Ca^{2+} release trace, Fig. 5f) statistically differed between the two groups. Mean values for maximum $d[Ca_{Tot}]/dt$ assessed from fitting a Boltzmann function to the voltage dependence of the peak $d[Ca_{Tot}]/dt$ in each fibre were 76.0 ± 6.5 and 78.1 ± 4.4 µmol l^{-1} ms^{-1} in the SCD and HFHSD groups, respectively. Thus, the physiological RYR1 channel activity and the SR Ca^{2+} content are preserved in HFHSD fibres.

Cytosolic Ca^{2+}removal capabilities and response to a fatiguing stimulation protocol Functional impact of HFD-induced obesity on SERCA activity may occur because of altered SR phospholipid composition [28, 29] and/or changes in expression or efficiency of the SERCA regulator sarcolipin [30]. SERCA is the major actor of cytosolic Ca^{2+} clearance. We assessed the cytosolic removal capabilities of fibres by measuring the time constant of the Ca^{2+} signal decay following repolarisation-induced Ca^{2+} release termination. For this we used the intermediate affinity Ca^{2+}-sensitive dye Fluo-4FF under non-EGTA-buffering conditions of the intracellular medium (see Methods: Buffers and incubation media). Illustrative Fluo-4FF Ca^{2+} transients elicited by maximum activation of SR Ca^{2+} under these conditions are presented in Fig. 6a. In each fibre tested, a single exponential function was fitted to the declining phase of the transients. Corresponding mean values for the time constant of decay showed no sign of any trend of difference between the two groups (Fig. 6b, data from eight fibres from four SCD mice and from 13 fibres from five HFHSD mice).

Under the same conditions, we explored the response of the fibres to an exhausting stimulation protocol consisting in consecutive trains of 30, 5-ms-long, pulses from −80 mV to +60 mV delivered at 100 Hz. Thirty trains were applied, separated by a 0.7 s interval. This protocol produces a rapid

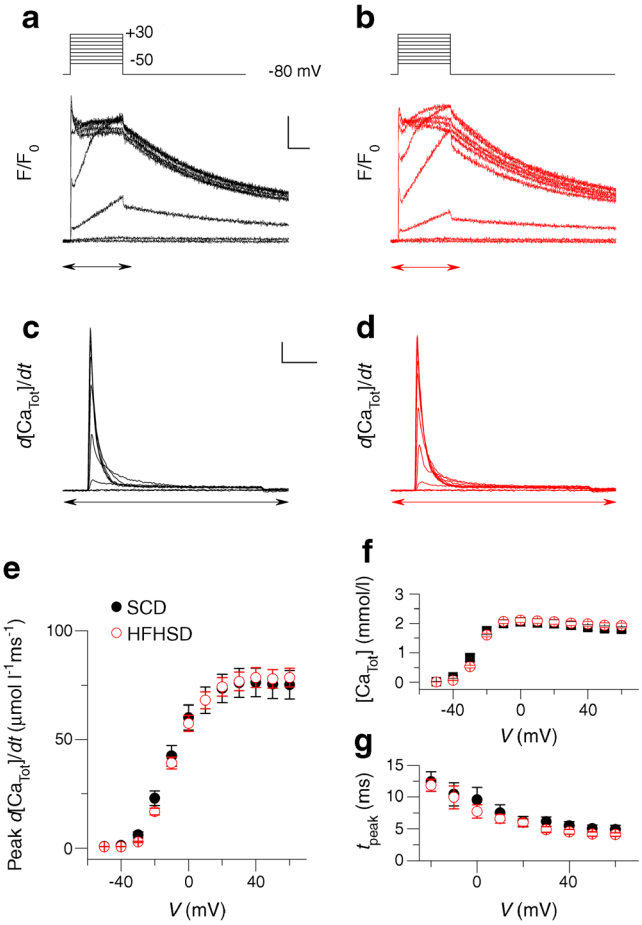

Fig. 5 Voltage-activated SR Ca^{2+} release. (**a**, **b**) Example traces of Rhod-2 F/F_0 Ca^{2+} transients in an SCD (**a**) and in an HFHSD muscle fibre (**b**) in response to the voltage-clamp pulse protocol shown at the top. Horizontal axis, time (scale bar 200 ms), vertical axis, fluorescence (scale bar 1×F_0). (**c**, **d**) Rate of SR Ca^{2+} release ($d[Ca_{Tot}]/dt$) calculated from the Rhod-2 transients shown in (**a**, **b**), respectively. Horizontal axis, time (scale bar 100 ms), vertical axis, rate of SR Ca^{2+} release (scale bar 10 μmol l^{-1} ms^{-1}). For the sake of clarity, the rate traces are only shown throughout the portion of Rhod-2 F/F_0 traces highlighted by an arrow in (**a**, **b**). (**e**) Mean values for the peak rate of SR Ca^{2+} release (peak $d[Ca_{Tot}]/dt$) vs voltage in the SCD ($n = 21$ fibres from 4 mice) and HFHSD ($n = 30$ fibres from 5 mice) groups. (**f**) Corresponding mean values for the total amount of released Ca^{2+} ($[Ca_{Tot}]$, calculated from the time integral of the rate). (**g**) Corresponding mean values for the time to peak SR Ca^{2+} release (t_{peak}). Data are mean ± SEM

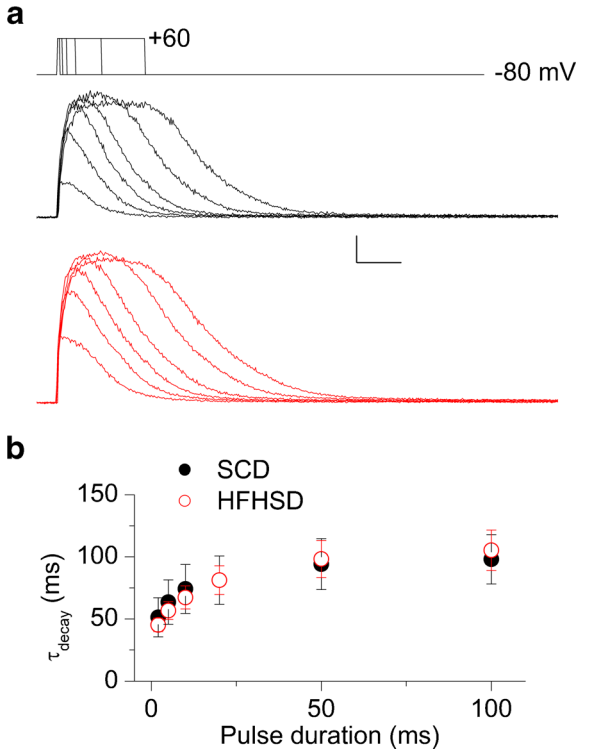

Fig. 6 Cytosolic Ca^{2+} removal. (**a**) Fluo-4FF F/F_0 Ca^{2+} transients elicited by the voltage-clamp pulse protocol shown on top in an SCD muscle fibre (top, black) and in an HFHSD muscle fibre (bottom, red). Horizontal axis, time (scale bar 50 ms), vertical axis, fluorescence (scale bar 5×F_0). (**b**) Mean values for the time constant of Fluo-4FF fluorescence decay (τ_{decay}) vs pulse duration in the SCD ($n = 8$ fibres from 4 mice) and HFHSD ($n = 13$ fibres from 5 mice) groups. Data are mean ± SEM

reduction of SR Ca^{2+} release as illustrated in Fig. 7a and b, which show examples of the first and last Fluo-4FF transients recorded from an SCD and from an HFHSD muscle fibre, respectively, in response to a full protocol. Figure 7c and d show the entire sequence of Fluo-4FF transients from the same two fibres over time. Such records were collected from eight fibres from four SCD mice and from 12 fibres from five HFHSD mice, respectively. Mean values for the normalised time course of decline of the peak F/F_0 transients in the two groups are presented in Fig. 7e. In each fibre, the time course was fitted by a single exponential plus constant function:

corresponding mean values for the time constant and final level (Fig. 7f, g) establish that there was no stringent alteration in HFHSD fibres. The time constant of decay was increased by a factor of ~1.25 in the HFHSD group, but the difference did not reach statistical significance ($p = 0.057$).

Spontaneous Ca^{2+} release activity at rest Spontaneous activity of RYR1 channels at rest under the form of local SR Ca^{2+} release events called Ca^{2+} sparks is a hallmark of several muscle disease situations [24, 31, 32]. We tested whether this was the case in HFHSD fibres using confocal imaging of the Ca^{2+}-sensitive dye Fluo-4: *x,y* images of the standard deviation of Fluo-4 fluorescence intensity along 30 consecutive confocal frames (total time of ~30 s) from an SCD fibre and from an HFHSD fibre are shown in Fig. 8a and b, respectively: SCD fibres were basically devoid of Ca^{2+} spark activity whereas some HFHSD fibres did exhibit a few sparks. Ca^{2+} spark activity was quantified in 28 muscle fibres from three SCD mice and from 46 fibres from five HFHSD mice, respectively. Figure 8c shows the mean value for relative fibre area exhibiting Ca^{2+} spark activity over a period of ~30 s (see Methods: Confocal imaging) in the two groups. Figure 8d shows the corresponding distribution of the number of fibres

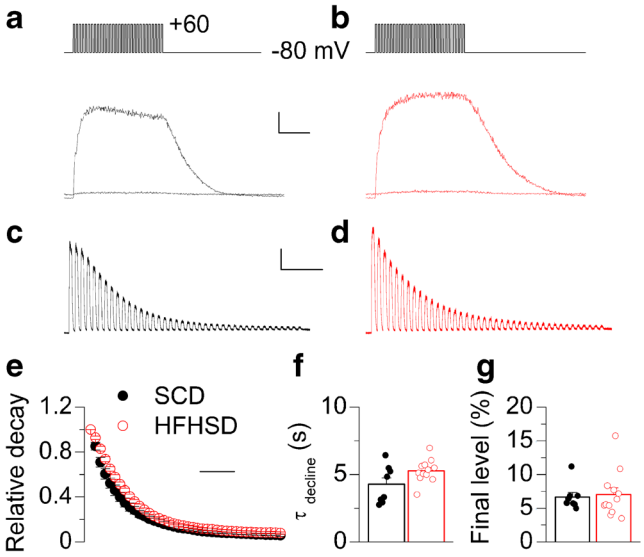

Fig. 7 Response to a fatigue protocol. (**a**, **b**) Representative Fluo-4FF fluorescence traces from an SCD (**a**) and from an HFHSD muscle fibre (**b**) challenged by the voltage-clamp depolarisation protocol shown at the top, consisting of 5-ms-long pulses from −80 mV to +60 mV delivered at 100 Hz. Horizontal axis, time (scale bar 100 ms), vertical axis, fluorescence (scale bar $5\times F_0$). This protocol was repeated 30 times: the two superimposed Fluo-4FF traces correspond to the responses to the first (largest) and to the last response of each fibre. (**c**, **d**) Full time course of the Fluo-4FF fluorescence transients over the course of the entire protocol (same muscle fibres as in **a** and **b**, respectively). Horizontal axis, time (scale bar 5 s), vertical axis, fluorescence (scale bar $5\times F_0$). (**e**) Mean time course of the decay of the relative peak Fluo-4FF Ca^{2+} transients over the full protocol. Horizontal axis, time (scale bar 5 s). (**f**, **g**) Mean values for the time constant of decay of the peak Fluo-4FF transients and corresponding final level, respectively, obtained from a single exponential plus constant fit to the data in each fibre ($n = 8$ fibres from 4 SCD mice and $n = 12$ fibres from 5 HFHSD mice). Data are mean ± SEM

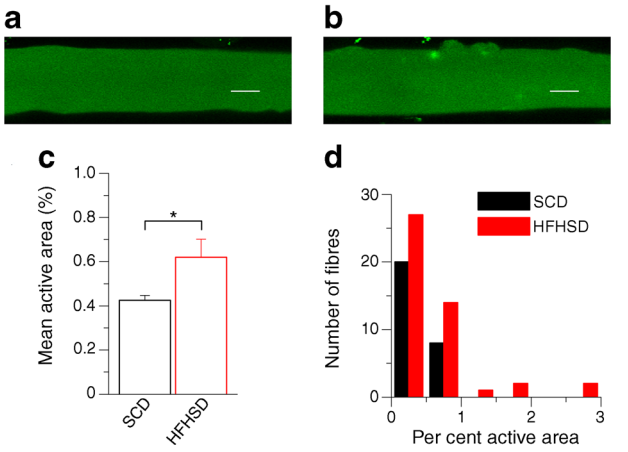

Fig. 8 Spontaneous Ca^{2+} spark activity at rest. (**a**, **b**) Images of the standard deviation of Fluo-4 fluorescence intensity in an SCD (**a**) and in an HFHSD muscle fibre (**b**) over the course of a series of 30 *x,y* confocal scans. Horizontal scale bar 10 μm. (**c**) Mean values for the relative fibre area exhibiting spontaneous Ca^{2+} release in SCD and HFHSD muscle fibres. (**d**) Corresponding distribution of the number of muscle fibres according to the relative active area. Ca^{2+} spark activity was quantified in 28 muscle fibres from three SCD mice and from 46 fibres from five HFHSD mice, respectively. Data are mean ± SEM. $^*p < 0.05$

according to this parameter. The mean fibre area exhibiting Ca^{2+} spark activity was significantly ($p = 0.043$) increased in the HFHSD group but in a quantitatively very modest manner (0.6% of the fibre area compared with 0.4% in the SCD group), this being essentially due to four muscle fibres issued from one HFHSD mouse, exhibiting an active relative fibre area larger than 1.5%.

Discussion

Altered skeletal muscle function associated with obesity and type 2 diabetes is a major burden for patients' mobility and locomotion (e.g. [33]). In the long run, muscle-extrinsic mechanisms related to cardiac and vascular complications obviously play a role and so does muscle atrophy. However, there is also evidence that muscle-intrinsic impaired force production is involved [2] but the underlying mechanisms remain obscure. HFD-induced obesity in mice is associated with reduced specific muscle force, prompting the interest of this model to decipher the muscle-intrinsic mechanisms. Intracellular Ca^{2+} plays a key role in numerous aspects of muscle function including triggering contraction. In order to ensure this particular function, intracellular Ca^{2+} concentration has to remain under tight control and, accordingly, there are numerous examples of muscle dysfunction due to altered Ca^{2+} handling and ECC (see [34–37]).

Defective Ca^{2+} regulation was previously suggested to occur in a pharmacologically induced diabetes model and in a genetically obese mouse model: specifically, accumulation of Ca^{2+} together with increased amount of $Ca_V1.1$ was shown in skeletal muscle from a rat model of streptozotocin-induced diabetes [38] and Ca^{2+} regulation was reported to be abnormal in the *ob/ob* mouse model of obesity, contributing to premature fatigue [39]. If referring specifically to HFD models, altered Ca^{2+} handling is suggested to play a role in obesity-induced muscle dysfunction through HFD-induced increased production of reactive oxygen species (ROS), which would promote SR Ca^{2+} leak through enhanced *S*-nitrosylation of RYR1 channels [40] and, possibly, also impair SERCA function [41, 42]. In addition, altered expression and/or efficiency of sarcolipin [30] could also contribute to impair cytosolic Ca^{2+} clearance, potentially with consequences for muscle metabolism and energy expenditure through activation of Ca^{2+} signalling pathways [43, 44]. Still, altogether, functional correlates for these alterations in terms of Ca^{2+} handling within the course of physiological ECC are poorly documented.

The strength of the present study is to achieve the first detailed quantitative investigation of the functional properties of intracellular Ca^{2+} handling and ECC in a diet-induced mouse model of obesity, using single isolated muscle fibres under voltage control. Our results demonstrate remarkably well preserved

Ca^{2+} handling capabilities in terms of voltage-dependent Ca^{2+} entry across the plasma membrane through $Ca_V1.1$, $Ca_V1.1$ properties as ECC voltage-sensors, voltage-activated SR Ca^{2+} release through RYR1 channels, SERCA-mediated cytosolic Ca^{2+} removal and resistance to a fatiguing stimulation protocol. Results concur with data from Eshima et al [6] suggesting that HFD elicits no change in the expression levels of calcium handling-related proteins, but they further show that the physiological operating function of these proteins during ECC is largely unaffected in that situation. They also concur with results from Bruton et al [39] showing that resting and tetanic Ca^{2+} under unfatigued conditions are similar in *ob/ob* and wild-type muscle fibres. Overall, our results do not exclude the possibility that the previously suggested, above-mentioned, alterations of Ca^{2+} handling do occur, but show that they remain very minor in terms of functional impact on the basic function of ECC and are thus not likely to be directly involved in chronic reduced muscle performance. For instance, the fact that some muscle fibres from HFHSD mice exhibit an enhanced propensity for spontaneous Ca^{2+} release at rest may be related to the presence of *S*-nitrosylated leaky RYR1 channels, but overall, this clearly does not compromise the SR Ca^{2+} content and proper function of the Ca^{2+} release machinery. It may then be that the reported alterations of Ca^{2+} homeostasis remain silent with regard to ECC function but relevant with regard to activation of specific Ca^{2+}-dependent signalling pathways. Also of importance, the preserved Ca^{2+} handling capabilities in isolated fibres maintained under our controlled experimental conditions do not eliminate the possibility that the situation differs in vivo, owing to the specific environment experienced by the fibres in the diseased organism. It will thus be of high interest in the future to investigate the function of ECC and Ca^{2+} handling in isolated fibres challenged by conditions mimicking this environment, including incubation of the fibres in the presence of insulin and glucose. In line with this, for instance, it is interesting that elevated glucose was recently reported to alter T-tubule morphology of isolated muscle fibres [26].

In summary, our results demonstrate that the intrinsic function of intracellular Ca^{2+} signalling and ECC is amazingly well preserved in muscle fibres from a mouse model of obesity and type 2 diabetes.

Data availability Original datasets and datasets generated by the described analysis procedures are available from the corresponding author upon reasonable request. Critical resources supporting the results are also available upon reasonable request.

Funding FJF was the recipient of a PhD fellowship from the Chilean Comisión Nacional de Investigación Científica y Tecnológica (CONYCIT). AB was supported by a research fellowship from the French Ministry of Higher Education and Research. This work was also supported by grants from CNRS, Inserm, the Université Claude Bernard - Lyon 1 to the Institut NeuroMyoGène and by the Chilean–French cooperation programme ECOS-CONICYT (#C13B01).

Authors' relationships and activities The authors declare that there are no relationships or activities that might bias, or be perceived to bias, their work.

Contribution statement VJ, JR and FJF conceived and coordinated the study. JR and AB generated the mouse model and collected metabolic data. FJF conducted the electrophysiological and fluorescence experiments. FJF, LM and VJ performed the main electrophysiological and fluorescence data analysis. All authors made critical contributions to data analysis, interpretation and discussion and to manuscript preparation, and approved the final version. VJ and JR wrote the manuscript.

VJ is the guarantor of this work and, as such, accepts full responsibility for the work and/or the conduct of the study, had access to the data, and controlled the decision to publish.

References

1. Allen MD, Doherty TJ, Rice CL, Kimpinski K (2016) Physiology in medicine: neuromuscular consequences of diabetic neuropathy. J Appl Physiol 121(1):1–6. https://doi.org/10.1152/japplphysiol.00733.2015
2. Tallis J, James RS, Seebacher F (2018) The effects of obesity on skeletal muscle contractile function. J Exp Biol 221(13):jeb163840. https://doi.org/10.1242/jeb.163840
3. King AJ (2012) The use of animal models in diabetes research. Br J Pharmacol 166(3):877–894. https://doi.org/10.1111/j.1476-5381.2012.01911.x
4. King A, Bowe J (2016) Animal models for diabetes: understanding the pathogenesis and finding new treatments. Biochem Pharmacol 99:1–10. https://doi.org/10.1016/j.bcp.2015.08.108
5. Matsakas A, Prosdocimo DA, Mitchell R et al (2015) Investigating mechanisms underpinning the detrimental impact of a high-fat diet in the developing and adult hypermuscular myostatin null mouse. Skelet Muscle 5(1):38. https://doi.org/10.1186/s13395-015-0063-5
6. Eshima H, Tamura Y, Kakehi S et al (2017) Long-term, but not short-term high-fat diet induces fiber composition changes and impaired contractile force in mouse fast-twitch skeletal muscle. Physiol Rep 5(7):e13250. https://doi.org/10.14814/phy2.13250
7. Tallis J, Hill C, James RS, Cox VM, Seebacher F (2017) The effect of obesity on the contractile performance of isolated mouse soleus, EDL, and diaphragm muscles. J Appl Physiol 122(1):170–181. https://doi.org/10.1152/japplphysiol.00836.2016
8. Leopoldo AS, Lima-Leopoldo AP, Sugizaki MM et al (2011) Involvement of L-type calcium channel and SERCA2a in myocardial dysfunction induced by obesity. J Cell Physiol 226(11):2934–2942. https://doi.org/10.1002/jcp.22643
9. Sánchez G, Araneda F, Peña JP et al (2018) High-fat-diet-induced obesity produces spontaneous ventricular arrhythmias and increases the activity of ryanodine receptors in mice. Int J Mol Sci 19(2):533. https://doi.org/10.3390/ijms19020533
10. Carvajal K, Balderas-Villalobos J, Bello-Sanchez MD et al (2014) Ca^{2+} mishandling and cardiac dysfunction in obesity and insulin resistance: role of oxidative stress. Cell Calcium 56(5):408–415. https://doi.org/10.1016/j.ceca.2014.08.003
11. Jia G, DeMarco VG, Sowers JR (2016) Insulin resistance and hyperinsulinaemia in diabetic cardiomyopathy. Nat Rev Endocrinol 12(3):144–153. https://doi.org/10.1038/nrendo.2015.216
12. Melzer W, Herrmann-Frank A, Lüttgau HC (1995) The role of Ca^{2+} ions in excitation–contraction coupling of skeletal muscle fibres. Biochim Biophys Acta 1241(1):59–116. https://doi.org/10.1016/0304-4157(94)00014-5
13. Rebbeck RT, Karunasekara Y, Board PG, Beard NA, Casarotto MG, Dulhunty AF (2014) Skeletal muscle excitation–contraction

coupling: who are the dancing partners? Int J Biochem Cell Biol 48: 28–38. https://doi.org/10.1016/j.biocel.2013.12.001
14. Hernández-Ochoa EO, Schneider MF (2018) Voltage sensing mechanism in skeletal muscle excitation–contraction coupling: coming of age or midlife crisis? Skelet Muscle 8(1):22. https://doi.org/10.1186/s13395-018-0167-9
15. Ríos E (2018) Calcium-induced release of calcium in muscle: 50 years of work and the emerging consensus. J Gen Physiol 150(4): 521–537. https://doi.org/10.1085/jgp.201711959
16. Bassel-Duby R, Olson EN (2006) Signaling pathways in skeletal muscle remodeling. Annu Rev Biochem 75(1):19–37. https://doi.org/10.1146/annurev.biochem.75.103004.142622
17. Gehlert S, Bloch W, Suhr F (2015) Ca^{2+}-dependent regulations and signaling in skeletal muscle: from electro-mechanical coupling to adaptation. Int J Mol Sci 16(1):1066–1095. https://doi.org/10.3390/ijms16011066
18. Eshima H, Poole DC, Kano Y (2014) In vivo calcium regulation in diabetic skeletal muscle. Cell Calcium 56(5):381–389. https://doi.org/10.1016/j.ceca.2014.08.008
19. Vial G, Chauvin MA, Bendridi N et al (2015) Imeglimin normalizes glucose tolerance and insulin sensitivity and improves mitochondrial function in liver of a high-fat, high-sucrose diet mice model. Diabetes 64(6):2254–2264. https://doi.org/10.2337/db14-1220
20. Jacquemond V (1997) Indo-1 fluorescence signals elicited by membrane depolarization in enzymatically isolated mouse skeletal muscle fibers. Biophys J 73(2):920–928. https://doi.org/10.1016/S0006-3495(97)78124-4
21. Collet C, Csernoch L, Jacquemond V (2003) Intramembrane charge movement and L-type calcium current in skeletal muscle fibers isolated from control and mdx mice. Biophys J 84(1):251–265. https://doi.org/10.1016/S0006-3495(03)74846-2
22. Pouvreau S, Allard B, Berthier C, Jacquemond V (2004) Control of intracellular calcium in the presence of nitric oxide donors in isolated skeletal muscle fibres from mouse. J Physiol 560(3):779–794. https://doi.org/10.1113/jphysiol.2004.072397
23. Horowicz P, Schneider MF (1981) Membrane charge movement in contracting and non-contracting skeletal muscle fibres. J Physiol 314(1):565–593. https://doi.org/10.1113/jphysiol.1981.sp013725
24. Kutchukian C, Szentesi P, Allard B et al (2017) Impaired excitation–contraction coupling in muscle fibres from the dynamin2R465W mouse model of centronuclear myopathy. J Physiol 595(24):7369–7382. https://doi.org/10.1113/JP274990
25. Grice BA, Barton KJ, Covert JD et al (2019) Excess membrane cholesterol is an early contributing reversible aspect of skeletal muscle insulin resistance in C57BL/6NJ mice fed a Western-style high-fat diet. Am J Phys 317(2):E362–E373. https://doi.org/10.1152/ajpendo.00396.2018
26. Hernández-Ochoa EO, Robison P, Contreras M, Shen T, Zhao Z, Schneider MF (2012) Elevated extracellular glucose and uncontrolled type 1 diabetes enhance NFAT5 signaling and disrupt the transverse tubular network in mouse skeletal muscle. Exp Biol Med 237(9):1068–1083. https://doi.org/10.1258/ebm.2012.012052
27. Llanos P, Contreras-Ferrat A, Georgiev T et al (2015) The cholesterol-lowering agent methyl-β-cyclodextrin promotes glucose uptake via GLUT4 in adult muscle fibers and reduces insulin resistance in obese mice. Am J Phys 308(4):E294–E305. https://doi.org/10.1152/ajpendo.00189.2014
28. Funai K, Song H, Yin L et al (2013) Muscle lipogenesis balances insulin sensitivity and strength through calcium signaling. J Clin Invest 123(3):1229–1240. https://doi.org/10.1172/JCI65726
29. Funai K, Lodhi IJ, Spears LD et al (2016) Skeletal muscle phospholipid metabolism regulates insulin sensitivity and contractile function. Diabetes 65(2):358–370. https://doi.org/10.2337/db15-0659
30. Paran CW, Verkerke AR, Heden TD et al (2015) Reduced efficiency of sarcolipin-dependent respiration in myocytes from humans with severe obesity. Obesity 23(7):1440–1449. https://doi.org/10.1002/oby.21123
31. Kutchukian C, Szentesi P, Allard B, Buj-Bello A, Csernoch L, Jacquemond V (2019) Ca^{2+}-induced sarcoplasmic reticulum Ca^{2+} release in myotubularin-deficient muscle fibers. Cell Calcium 80: 91–100. https://doi.org/10.1016/j.ceca.2019.04.004
32. Lotteau S, Ivarsson N, Yang Z et al (2019) A mechanism for statin-induced susceptibility to myopathy. JACC Basic Transl Sci 4(4): 509–523. https://doi.org/10.1016/j.jacbts.2019.03.012
33. Bianchi L, Volpato S (2016) Muscle dysfunction in type 2 diabetes: a major threat to patient's mobility and independence. Acta Diabetol 53(6):879–889. https://doi.org/10.1007/s00592-016-0880-y
34. Ríos E, Figueroa L, Manno C, Kraeva N, Riazi S (2015) The couplonopathies: a comparative approach to a class of diseases of skeletal and cardiac muscle. J Gen Physiol 145(6):459–474. https://doi.org/10.1085/jgp.201411321
35. Allard B (2018) From excitation to intracellular Ca^{2+} movements in skeletal muscle: basic aspects and related clinical disorders. Neuromuscul Disord 28(5):394–401. https://doi.org/10.1016/j.nmd.2018.03.004
36. Avila G (2018) Disturbed Ca^{2+} homeostasis in muscle-wasting disorders. Adv Exp Med Biol 1088:307–326. https://doi.org/10.1007/978-981-13-1435-3_14
37. Denniss A, Dulhunty AF, Beard NA (2018) Ryanodine receptor Ca^{2+} release channel post-translational modification: central player in cardiac and skeletal muscle disease. Int J Biochem Cell Biol 101: 49–53. https://doi.org/10.1016/j.biocel.2018.05.004
38. Ogawa T, Kashiwagi A, Kikkawa R, Shigeta Y (1995) Increase of voltage-sensitive calcium channels and calcium accumulation in skeletal muscles of streptozocin-induced diabetic rats. Metabolism 44(11):1455–1461. https://doi.org/10.1016/0026-0495(95)90146-9
39. Bruton JD, Katz A, Lännergren J, Abbate F, Westerblad H (2002) Regulation of myoplasmic Ca^{2+} in genetically obese (*ob/ob*) mouse single skeletal muscle fibres. Pflugers Arch 444(6):692–699. https://doi.org/10.1007/s00424-002-0882-1
40. Jain SS, Paglialunga S, Vigna C et al (2014) High-fat diet-induced mitochondrial biogenesis is regulated by mitochondrial-derived reactive oxygen species activation of CaMKII. Diabetes 63(6): 1907–1913. https://doi.org/10.2337/db13-0816
41. Matsunaga S, Inashima S, Yamada T, Watanabe H, Hazama T, Wada M (2003) Oxidation of sarcoplasmic reticulum Ca^{2+}-ATPase induced by high-intensity exercise. Pflugers Arch 446(3): 394–399. https://doi.org/10.1007/s00424-003-1040-0
42. Vázquez P, Tirado-Cortés A, Álvarez R, Ronjat M, Amaya A, Ortega A (2016) Reversible oxidation of vicinal-thiols motif in sarcoplasmic reticulum calcium regulatory proteins is involved in muscle fatigue mechanism. Cell Calcium 60(4):245–255. https://doi.org/10.1016/j.ceca.2016.06.001
43. Maurya SK, Bal NC, Sopariwala DH et al (2015) Sarcolipin is a key determinant of the basal metabolic rate, and its overexpression enhances energy expenditure and resistance against diet-induced obesity. J Biol Chem 290(17):10840–10949. https://doi.org/10.1074/jbc.M115.636878
44. Maurya SK, Herrera JL, Sahoo SK et al (2018) Sarcolipin signaling promotes mitochondrial biogenesis and oxidative metabolism in skeletal muscle. Cell Rep 24(11):2919–2931. https://doi.org/10.1016/j.celrep.2018.08.036